The Effect of a Pressure-Containing Correlation Model on Near-Wall Flow Simulations With Reynolds Stress Transport Models

Svetlana V. Poroseva
Assistant Professor
Department of Mechanical Engineering,
The University of New Mexico,
Albuquerque, NM 87131-0001
e-mail: poroseva@unm.edu

It is accustomed to think that turbulence models based on solving the Reynolds-averaged Navier–Stokes (RANS) equations require empirical functions to accurately reproduce the behavior of flow characteristics of interest, particularly near a wall. The current paper analyzes how choosing a model for pressure-strain correlations in second-order closures affects the need for introducing empirical functions in model equations to reproduce the flow behavior near a wall correctly. An axially rotating pipe flow is used as a test flow for the analysis. Results of simulations demonstrate that by using more physics-based models to represent pressure-strain correlations, one can eliminate wall functions associated with such models. The higher the Reynolds number or the strength of imposed rotation on a flow, the less need there is for empirical functions regardless of the choice of a pressure-strain correlation model. [DOI: 10.1115/1.4025936]

1 Introduction

The solution of the Navier–Stokes equations describes a turbulent flow structure anywhere in the flow, including near-wall areas. Such solutions can be obtained using direct numerical simulations (DNS) of the Navier–-Stokes equations. However, DNS are computationally infeasible for flow simulations at high Reynolds numbers that are of interest for industrial applications.

A statistically equivalent alternative to DNS is solving the full set of the RANS equations, which includes transport equations for all statistical moments (velocity correlations). The knowledge of all statistical moments is equivalent to the knowledge of the probability density function of a random field [1]. Therefore, a turbulent flow structure can also be completely described in the same way. The problem is that in a general case the full set includes an infinite number of RANS equations, which makes it impossible to find a solution.

To make the RANS approach practical, one uses a procedure called "closure." In this procedure, the full set of RANS equations is reduced to include only transport equations for velocity correlations of a specified order and below. Such equations contain velocity correlations of higher orders. To exclude them from the list of unknown parameters, higher-order velocity correlations are modeled in terms of a chosen set of lower-order turbulence statistics. The result is a closed set of modeled RANS equations that includes transport equations for velocity correlations of the specified order and below. More on the philosophy of the closure procedure and history of its development can be found in Refs. [1,2].

The highest order of velocity correlations that transport equations are solved for provides a basis for categorizing a closure as first, second, and so on order. For example, all one- and two-equation RANS models that are typically used in the industry fall into the category of first-order closures because from all possible RANS equations such models only solve the equations for mean velocity components. In second-order RANS closures, transport equations for third- and higher-order velocity correlations are cut off from the set of solved equations.

When compared to a full set of exact RANS equations, closures of any order do not accurately reproduce the flow physics. However, this is acceptable as long as the behavior of the flow characteristics of interest is reproduced correctly. One verifies whether this requirement is met by comparing the results of simulations conducted with a chosen RANS model with a reliable experimental database. Unfortunately, no such database exists for many flows of practical importance.

Another indicator that a RANS model substantially lacks the capability to correctly reproduce the required flow physics is the model's need for empirical functions/corrections. Such a need is usually revealed in simulations of benchmark flows with an existing experimental database. Although empirical functions facilitate simulations, ultimately, their presence in equations is undesirable due to their unphysical nature. The development of RANS models that are free from empirical functions is the ultimate goal of our research.

To achieve this goal, sources of deficiencies in modeled RANS equations should be identified and analyzed. Of all RANS models, the first-order closures are the least accurate models to compare with the full set of exact RANS equations because of their formulation. Indeed, all effects due to turbulence are modeled in these closures. As a result, empirical functions are unavoidable in such models. Even with empirical functions, these models do not adequately describe flow physics in near-wall areas of complex flows (see discussion in Refs. [3–5]). In some wall flows, it was analytically shown [6] that first-order closures could not generate the correct solution even for the mean velocity components.

Second- and higher-order closures solve transport equations for turbulence statistical characteristics, and therefore, have more potential for improving the description of flow behavior everywhere, including in near-wall areas [2,7].

It was previously shown [8,9] that modeled RANS equations for third- and fourth-order velocity correlations seem capable of accurately reproducing the behavior of corresponding velocity correlations throughout the flow area, including near a wall, without any empirical functions. Therefore, the focus of our research

Contributed by the Fluids Engineering Division of ASME for publication in the Journal of Fluids Engineering. Manuscript received April 22, 2013; final manuscript received October 28, 2013; published online April 28, 2014. Assoc. Editor: Ye Zhou.

is an analysis of deficiencies in second-order closures or the Reynolds stress transport models (hereafter, RST models).

In RST models, the main sources of deficiencies are model expressions used to represent three of the terms in the exact RANS equation for Reynolds stresses:

$$\frac{\partial\langle u_i u_j\rangle}{\partial t}+U_k\frac{\partial\langle u_i u_j\rangle}{\partial x_k}=-\langle u_i u_k\rangle\frac{\partial U_j}{\partial x_k}-\langle u_j u_k\rangle\frac{\partial U_i}{\partial x_k}+\nu\frac{\partial^2\langle u_i u_j\rangle}{\partial x_k\partial x_k}+D_{ij}+\Pi_{ij}-\varepsilon_{ij} \tag{1}$$

These terms are turbulent diffusion D_{ij}, velocity–pressure-gradient correlations Π_{ij}, and dissipation tensor ε_{ij}defined as

$$D_{ij}=\frac{\partial\langle u_i u_j u_k\rangle}{\partial x_k},\ \Pi_{ij}=-\frac{1}{\rho}\left(\left\langle u_i\frac{\partial p}{\partial x_j}\right\rangle+\left\langle u_j\frac{\partial p}{\partial x_i}\right\rangle\right),\ \varepsilon_{ij}=2\nu\left\langle\frac{\partial u_i}{\partial x_k}\frac{\partial u_j}{\partial x_k}\right\rangle \tag{2}$$

The following notations are used in Eqs. (1) and (2), and hereafter: U_i and u_i are the mean and fluctuating velocity components, respectively; $\langle\ldots\rangle$ denotes the ensemble average; ρ is the density; p is the pressure fluctuation; and ν is the kinematic viscosity. In this paper, all equations are written using Cartesian notations to simplify presentation. In simulations, however, equations were written in cylindrical coordinates, as they are more relevant to test flow geometry. The exact RANS equations for velocity correlations of any order written in cylindrical coordinates can be found in Ref. [9].

The effect of modeling the turbulent diffusion term on the results of simulations in a rotating circular pipe flow was studied in Ref. [10]. It was found that the model choice for the turbulent diffusion term has a profound effect on the behavior of second-order velocity correlations everywhere in the flow, including in near-wall areas. It was shown that simulation results could be improved substantially by choosing a tensor-invariant turbulent diffusion model. It was also observed, that modeling velocity–pressure-gradient correlations had a much stronger effect on mean velocity profiles than modeling the turbulent diffusion. The current paper investigates further detail on the effects of modeling velocity–pressure-gradient correlations on the results of simulations. Particularly, the ability of the various models for these correlations to accurately reproduce new-wall flow behavior is analyzed. The effects of modeling the dissipation tensor, although highly important, are not considered in this paper.

To maintain consistency with previous works [8–10], a turbulent flow in an axially rotating circular pipe was chosen as the test flow. This is a wall-bounded flow with complex physics that relates to various engineering flows with boundary layers on a rotating surface, such as for example, flows in heat exchangers and rotor cooling systems.

2 RST Models

To analyze the effect of different velocity–pressure-gradient correlations models on simulation results, one has to keep models for turbulent diffusion terms and dissipation tensor unchanged in RST equations. The simplest models can be used in such an analysis. For turbulent diffusion terms, the Daly–Harlow model [11]

$$\langle u_i u_j u_k\rangle=-C_{s1}\tau\langle u_m u_k\rangle\frac{\partial\langle u_i u_j\rangle}{\partial x_m} \tag{3}$$

is used in the current study. In Eq. (3), $C_{s1}=0.18$, τ is a time scale defined as k/ε, and ε is the dissipation rate of turbulent kinetic energy k. The dissipation tensor ε_{ij} is modeled using an isotropic expression with a correction for the low Reynolds numbers near a solid wall [12]:

$$\varepsilon_{ij}=\frac{2}{3}\delta_{ij}\varepsilon+2\nu\frac{\langle u_i u_j\rangle}{x_n^2} \tag{4}$$

In Eq. (4), x_n is the normal distance to a wall and δ_{ij} is the Kronecker δ tensor. The transport equation for the dissipation rate of turbulent kinetic energy is used in the following form:

$$\frac{\partial\varepsilon}{\partial t}+U_k\frac{\partial\varepsilon}{\partial x_k}=\frac{\partial}{\partial x_k}\left[\left(\nu\delta_{jk}+C_\varepsilon\tau\langle u_j u_k\rangle\right)\frac{\partial\varepsilon}{\partial x_j}\right]+\frac{1}{\tau}\left(C_{\varepsilon1}P-C^*_{\varepsilon2}\varepsilon\right)-\frac{2\nu\varepsilon}{x_n^2}f_1 \tag{5}$$

Here, $2P=-\langle u_i u_k\rangle\partial U_i/\partial x_k$, $C^*_{\varepsilon2}=C_{\varepsilon2}f_2$ in a stationary pipe and $C^*_{\varepsilon2}=\max[1.4,C_{\varepsilon2}f_2]$ in a rotating pipe, and $C_{\varepsilon2}=11/6$. The values of coefficients C_ε and $C_{\varepsilon1}$ depend on the model choice for pressure-containing correlations. Damping functions f_1 and f_2 are defined as in Ref. [12]: $f_1=\exp[-x_n u_\tau/(2\nu)]$ and $f_2=1-2/9\cdot\exp\{-[k^2/(6\nu\varepsilon)]^2\}$, with u_τ being the friction velocity. Our choice of a model for the dissipation tensor and the model equation for ε is based on the results of our previous studies in the test flow geometry [10].

Even though a more physics-based model for the dissipation tensor is desirable, it was found previously [10,13] that the presence of the damping functions in Eq. (5) was not influenced by models for turbulent diffusion and pressure-containing correlations. It was also shown that the combination of Eqs. (4) and (5) provides stable computational solutions at various combinations of the Reynolds number $\mathrm{Re}=U_0D/\nu$, and the rotation rate $N=W_0/U_0$, where W_0 is the maximum circumferential mean velocity component (at the pipe wall), U_0 is the maximum axial mean velocity component (at the pipe centerline), and D is the pipe diameter. The computational step size in the axial direction can also be significantly increased when Eqs. (4) and (5) are used to model the dissipation tensor [13,14]. The issue of computational time becomes important when more complex models for pressure-containing correlations are implemented in RST equations.

Equation (1) contains a velocity–pressure-gradient correlations tensor (2) that has to be modeled. However, the usual practice would be to model a different tensor, the pressure-strain correlation tensor:

$$\Phi_{ij}=\frac{1}{\rho}\left(\left\langle p\frac{\partial u_i}{\partial x_j}\right\rangle+\left\langle p\frac{\partial u_j}{\partial x_i}\right\rangle\right) \tag{6}$$

This tensor can be obtained from the velocity–pressure-gradient correlation tensor by splitting the later into two parts: the pressure-strain correlations tensor Φ_{ij} and the pressure diffusion tensor $-1/\rho\cdot\left(\partial\langle pu_i\rangle/\partial x_j+\partial\langle pu_j\rangle/\partial x_i\right)$. The pressure diffusion tensor is usually neglected or assumed to be absorbed in a model for turbulent diffusion.

This practice of modeling pressure-containing correlations can be traced back to Rotta's work [15]. The consequences of its implementation in RST equations were analyzed in Refs. [16–18]. In the current paper, this practice is also adopted because we wish to analyze the improvement in flow simulations that can be achieved within the standard modeling framework.

Based on the results of our previous research [13], the following models for the pressure-strain correlations tensor were chosen for testing: isotropization-of-production (IP) and Launder-Reece-Rodi (LRR) models [19], linearized [20] and nonlinear [21] Speziale-Sarkar-Gatskii (SSG) models, and a structure-based Q-model [14,22]. The IP model is the simplest of the five models. The LRR model is the model that is most frequently implemented in various software. The Q-model is the most complex of the five models.

Table 1 Coefficients in the Φ_{ij}-models

	C_1	C_1^*	C_2	C_3	C_3^*	C_4	C_5
IP	3.6	0	0	0.8	0	1.2	1.2
LRR	3.6	0	0	0.8	0	1.75	1.31
LSSG	3.4	1.8	0	0.36	0	1.25	0.4
SSG	3.4	1.8	4.2	0.8	1.3	1.25	0.4

The IP, LRR, linearized SSG (hereafter, LSSG), and nonlinear SSG models can be represented by the same expression:

$$\Phi_{ij} = -\left(C_1\varepsilon + 2C_1^*P\right)b_{ij} + C_2\varepsilon\left(b_{ik}b_{kj} - \frac{1}{3}b_{kl}b_{kl}\delta_{ij}\right) + \left(C_3 - C_3^*\sqrt{b_{kl}b_{kl}}\right)kS_{ij} + C_4k\left(b_{ik}S_{jk} + b_{jk}S_{ik} - \frac{2}{3}b_{kl}S_{kl}\delta_{ij}\right) + C_5k\left(b_{ik}\Omega_{jk} + b_{jk}\Omega_{ik}\right) \quad (7)$$

where $b_{ij} = 1/2\left(\langle u_iu_j\rangle/k - 2\delta_{ij}/3\right)$, $S_{ij} = \left(U_{i,j} + U_{j,i}\right)/2$, and $\Omega_{ij} = \left(U_{i,j} - U_{j,i}\right)/2$. The model coefficients are given in Table 1. Notice that for the LRR model, a value of C_1 differs from its standard value of 3.0 [7]. It was found that simulation results fit closer experimental data with the value of this coefficient being 3.6.

The Q-model does not solve for a modeled form of Eq. (1), and thus, no direct modeling of pressure-containing correlations is involved. All nonlocal effects (including those of pressure fluctuations) are accounted for by additional structure tensors such as dimensionality, circulicity, and stropholysis Q_{ijk} [14,22]. The first two tensors are of the second rank; the stropholysis is the third-rank tensor. Instead of using Eq. (1), the stropholysis tensor transport equation is modeled and solved. Reynolds stresses are reconstructed from the components of the stropholysis tensor using the following relation: $R_{ij} = \varepsilon_{imp}Q_{jpm}$, where $\varepsilon_{ijk}$is the Levi–Civita tensor. The Q-model was included in the analysis because it aims to reproduce Reynolds stresses and, thus, falls into the category of second-order RANS closures. Due to the lack of an explicit model expression for pressure-containing correlations and the longevity and complexity of the Q-equations set, a reader is referred to Ref. [13] where Q-equations are given in detail.

The full set of Q-model equations also includes transport equations for the dissipation rate of turbulent kinetic energy (5). The turbulent diffusion of the Q-tensor is modeled using an expression similar to Eq. (3):

$$Q_{ijkn} = -C_Q\tau_Q\langle u_mu_n\rangle\frac{\partial Q_{ijk}}{\partial x_m} \quad (8)$$

[13], where $C_Q = 0.22$ and $\tau_Q = \sqrt{(k/\varepsilon)^2 + 36\nu/\varepsilon}$.

The performance of the five RST models was analyzed in the current study. The four RST models solve Eq. (1), with the turbulent diffusion, the dissipation tensor, and the pressure-strain correlations being modeled using expressions (3)–(5) and (7), along with one of the four sets of the model coefficients in Table 1. Depending on the chosen set of model coefficients in Table 1, RST models are labeled as IP, LRR, LSSG, or SSG. The Q-model is the fifth RST model used in the analysis. The coefficients C_ε and $C_{\varepsilon 1}$ in transport equation (5) for ε are 0.18 and 1.54, respectively, for all models except the Q-model where values are 0.22 and 1.5, respectively.

3 Numerical Procedure

Simulation conditions closely reproduced those in experiments [19,20]. In the first step, a fully developed turbulent flow was obtained at the exit of the stationary cylindrical pipe section. Then, the flow was conveyed into a cylindrical pipe section of the same diameter with rotation imposed on the flow by the rotating pipe wall (Fig. 1).

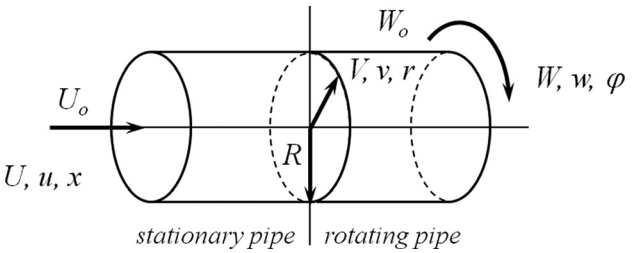

Fig. 1 Test flow geometry

Simulations were conducted at two Reynolds numbers: $Re = 2\times10^4$ and 4×10^4, with Re defined as previously: $\mathrm{Re} = U_0D/\nu$. The rotation strength that was imposed on the flow is characterized by the rotation rate $N = W_0/U_0$, and varied from 0 (no rotation) to 1 (strong rotation).

Equations used in simulations were written using boundary layer approximations in the axisymmetric cylindrical frame of reference $x^i = (x, r, \varphi)$, where x, r, and φ are the axial, radial, and angular coordinates, respectively (Fig. 1). In such coordinates, the covariant and contravariant components of velocity are $U_i = (U, V, rW)$ and $U^i = (U, V, W/r)$. Instead of equations for the individual turbulent kinetic energy components, equations for the turbulent kinetic energy k, $\langle u^2\rangle$, and $\langle w^2\rangle - \langle v^2\rangle$ were solved in the IP, LRR, SSG, and LSSG models. These equations provide the same information about the behavior of individual turbulent kinetic energy components but require simpler boundary conditions. The control volume technique [23] was used to solve the transport equations.

The grid was nonuniform in the radial direction, with the total number of nodes in this direction being 69 at $\mathrm{Re} = 2\times10^4$ for all models. At $\mathrm{Re} = 4\times10^4$, the number of nodes was 128 for all models except the Q-model. For the Q-model, the number of nodes was 65. Five nodes were uniformly placed within $y_+ \le 5$ at $\mathrm{Re} = 2\times10^4$ and at $\mathrm{Re} = 4\times10^4$ for the Q-model. At $\mathrm{Re} = 4\times10^4$, 10 nodes were uniformly placed within the same area for the other four RST models. In the test flow geometry, y_+ is defined as $y_+ = (1 - r/R)\mathrm{Re}_\tau$, where $\mathrm{Re}_\tau = (u_\tau R)/\nu$.

The number of nodes was determined by analyzing the solution convergence for each model. That is, at higher Re, the solution for the Q-model converged on the grid coarser than those used in simulations with the other models. The computational step in the axial direction was $0.001\,R$.

Boundary conditions for the IP, LRR, SSG, and LSSG models were the following:

$$\frac{\partial U}{\partial r} = \frac{\partial k}{\partial r} = \frac{\partial \varepsilon}{\partial r} = \frac{\partial\langle u^2\rangle}{\partial r} = \frac{\partial(\langle w^2\rangle - \langle v^2\rangle)}{\partial r} = \langle uv\rangle = \langle vw\rangle = \langle uw\rangle = W = 0$$

at the pipe centerline ($r = 0$) and

$$U = k = \varepsilon = \langle u^2\rangle = \langle w^2\rangle - \langle v^2\rangle = \langle uv\rangle = \langle vw\rangle = \langle uw\rangle = 0, \quad W = W_0$$

on the pipe wall at $r = R$.

For the Q-model, the boundary conditions at $r = 0$ were

$$\frac{\partial U}{\partial r} = \frac{\partial \varepsilon}{\partial r} = W = 0, \quad \frac{\partial Q_{ijk}}{\partial r} = 0, \quad \text{if} \quad i \ne j \ne k, \quad \text{and}$$
$$Q_{ijk} = 0, \quad \text{if} \quad i = j, \quad \text{or} \quad j = k, \quad \text{or} \quad i = k$$

At the wall, $U = Q_{ijk} = 0$ and $W = W_0$. More detail on the boundary conditions for the Q-model can be found in Ref. [13].

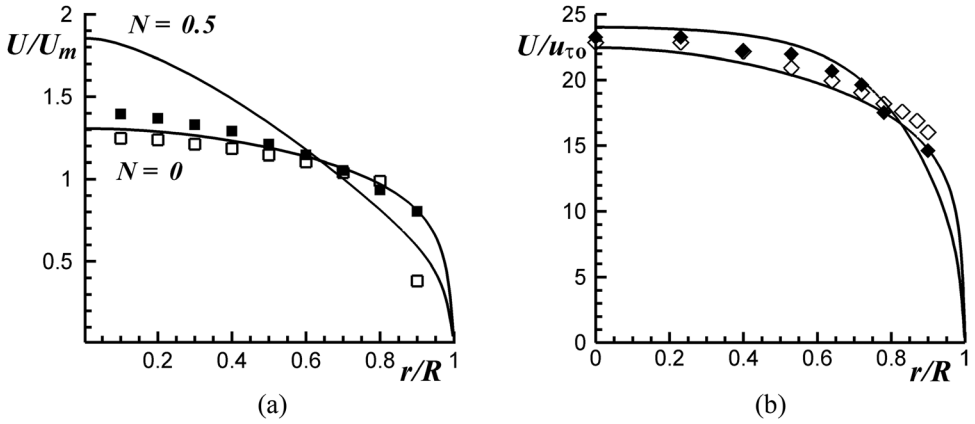

Fig. 2 The axial mean velocity component of the IP-model at (*a*) $Re = 2\times10^4$ and (*b*) $Re = 4\times10^4$. Notations: IP model: —; experiments: (*a*) □ $N = 0$, ■ $N = 0.5$ [27] and (*b*) ◇ $N = 0$, ◆ $N = 0.6$ [25].

For the IP model, initial conditions at the inlet of the stationary pipe section were the same as in Ref. [11]:

$$k(r) = k_0 = 10^{-3}u_\tau^2, \quad \langle u^2\rangle = (2/3)k_0,$$
$$\langle w^2\rangle - \langle v^2\rangle = 0, \quad \langle uv\rangle = 0$$
$$U(r) = \begin{cases} u_\tau y_+, & 0 \le y_+ \le A^{7/6}, \quad A = 8.74 \\ Au_\tau(y_+)^{1/7}, & A^{7/6} < y_+ \le \mathrm{Re}_\tau \end{cases}$$
$$\varepsilon(r) = \left(c_\mu f_\mu\right)^{1/2} k_0 \frac{\partial U}{\partial r}, \quad f_\mu = 1 - \exp(-0.01y_+), \quad c_\mu = 0.09$$

For the other models, IP-model profiles for U, Reynolds stresses, and ε at the stationary pipe section exit were used as the initial profiles to reduce the time of computations. The Q-model requires initial profiles for many other parameters. They are discussed in detail in Ref. [13].

4 Results

In the test flow, simulations should accurately reproduce the effects of the pipe wall and the pipe wall rotation on the behavior of the mean velocity components and the Reynolds stresses. In particular, experimental studies [24–27] established the existence of three regions along the rotating pipe section at a given rotation rate where rotation has a dramatically different effect on turbulence:

— the initial region where strong turbulence suppression is observed
— the transitional region where turbulence statistics tend to recover
— the final region where turbulence statistics are stabilized at some level just slightly lower than in the stationary pipe section

The initial region is relatively short, about $30D$. The final region is a region of fully developed turbulence that is observed at about $170D$ at any Reynolds number considered in experiments [24,27]. Similar dynamics of turbulence statistics was observed in the given pipe section by increasing the rotation rate [25].

Mean velocity components respond differently to rotation than turbulence statistics. Specifically, mean velocity component profiles are transformed along the pipe tending to shapes expected in a laminar flow but never reaching those limits. The fully developed profiles of the mean velocity components occur at approximately the same distance as the fully developed profiles of turbulence statistics [24,25,27].

Being the simplest of the considered RST models, the IP model also has the most difficulty reproducing the experimental results without additional corrections implemented in the Φ_{ij}-model. At $\mathrm{Re} = 2 \times 10^4$, strong disagreement with experimental data [28] is observed (Fig. 2(*a*)). Rotation enhances this disagreement. At higher Re ($\mathrm{Re} = 4 \times 10^4$), the need for corrections diminishes (Fig. 2(*b*)). Corrections are also required to accurately predict the

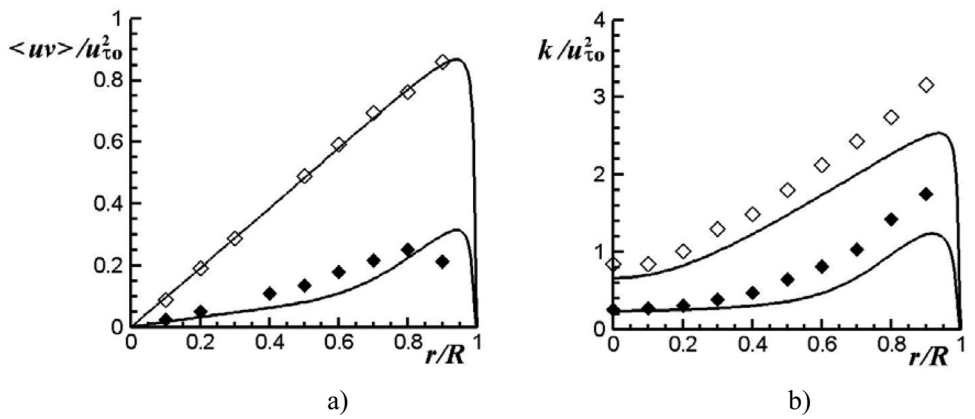

Fig. 3 The IP-model profiles of (*a*) shear stress and (*b*) turbulent kinetic energy calculated at $Re = 4\times10^4$ (see notations in Fig. 2(*b*))

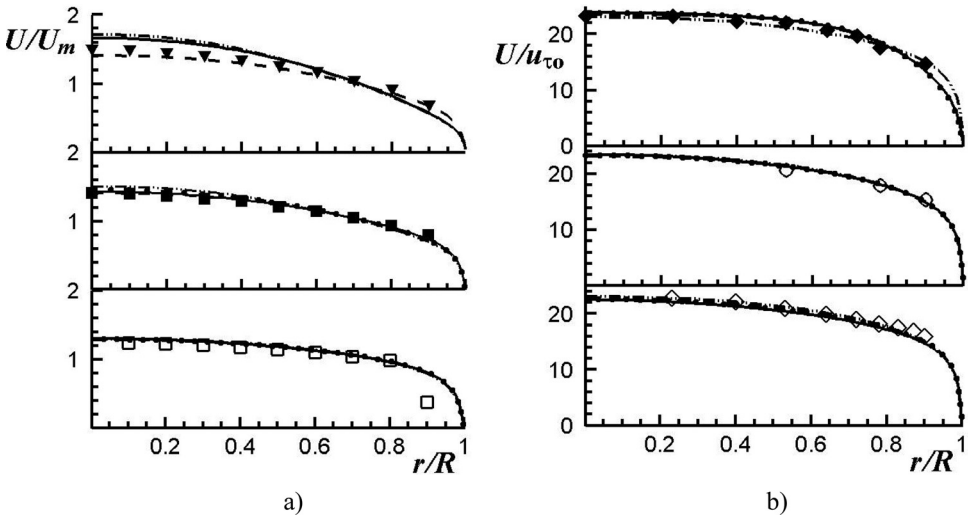

Fig. 4 The axial mean velocity components for LRR —, LSSG - - - -, SSG · · · · · · ·, and Q- — · · — models calculated at (*a*) $Re = 2\times10^4$ and (*b*) $Re = 4\times10^4$. Experiments: (*a*) □ $N = 0$, ■ $N = 0.5$, ▼ $N = 1$ [27] and (*b*) ◇ $N = 0$, ○ $N = 0.15$, ◆ $N = 0.6$ [25].

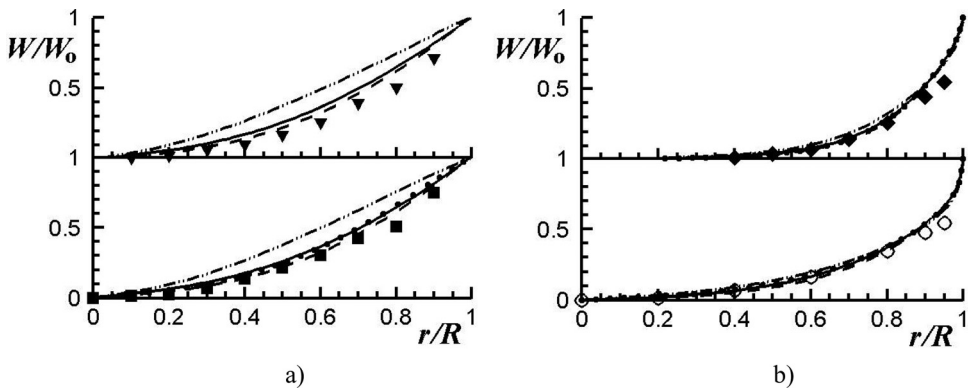

Fig. 5 The circumferential mean velocity components at (*a*) $Re = 2\times10^4$ and (*b*) $Re = 4\times10^4$ (see notations in Fig. 4)

shear stress $\langle uv \rangle$ and the turbulent kinetic energy k (Fig. 3). The shear stress in the stationary pipe section is correctly reproduced with the IP model without corrections. In the figures, R denotes the pipe radius; U_m is the bulk velocity and $u_{\tau 0}$ is the friction velocity at the pipe wall at the exit of the stationary pipe section, respectively.

Mean velocity profiles calculated in the other four models are shown in Figs. 4 and 5. These models are capable of reproducing the axial mean velocity profile at the stationary pipe section exit. They also successfully predict the transformation of the axial mean velocity profile under small to medium rotation rates ($N < 1$). The smaller Re and the higher N, the more the simulation results deviate from experimental data. Under strong rotation ($N = 1$), all models produce results that are far from experimental data (not shown here).

The circumferential velocity profiles are more sensitive to modeling pressure-strain correlations (Fig. 5). The Q-model fails to reproduce the transformation of W under rotation at $\mathrm{Re} = 2 \times 10^4$ (Fig. 5(*a*)). Results produced with other models are closer to the experimental data. At the medium rotation rate ($N = 0.6$), profiles obtained for all models deviate from the experimental data (Fig. 5(*a*)). It was shown in Ref. [13] that additional corrections that were introduced into the models did not improve results.

By increasing the Reynolds number ($\mathrm{Re} = 4 \times 10^4$), there is a decrease in the circumferential velocity component's dependence on the choice of the Φ_{ij}-model (Fig. 5(*b*)). At this Re, rotation also has less of an effect on agreement between the simulation results and the experimental data.

Simulation profiles obtained for the shear stress and turbulent kinetic energy of the four models are shown in Figs. 6–10. At $\mathrm{Re} = 2 \times 10^4$, all models overpredict the shear stress (Fig. 6(*a*)) in stationary and rotating pipe sections. At $\mathrm{Re} = 4 \times 10^4$, the results are in strong agreement with the experimental data (Fig. 6(*b*)). No wall corrections are necessary to reproduce the shear stress at this Re in the stationary pipe section. Under rotation, differences between the calculated and experimental profiles become noticeable in the near-wall area. This difference, however, can be eliminated by choosing a tensor-invariant turbulent diffusion model as shown in Ref. [10].

A choice of a turbulent diffusion model is also important for predicting turbulent kinetic energy at lower Re. With model (3), all considered RST models overpredict the turbulent kinetic energy level in the fully developed turbulence region of the rotating pipe section. Moreover, they predict it to be larger than in the stationary pipe. This contradicts experimental observations. Figure 7(*a*) illustrates this issue for the LRR model at $N = 0.5$. In the figure, the experimental profile at $N = 0.5$ lies below the profile measured at $N = 0$. The simulation results show the opposite tendency. Other models predict results similar to those obtained with the LRR model. Therefore, results for all models are shown

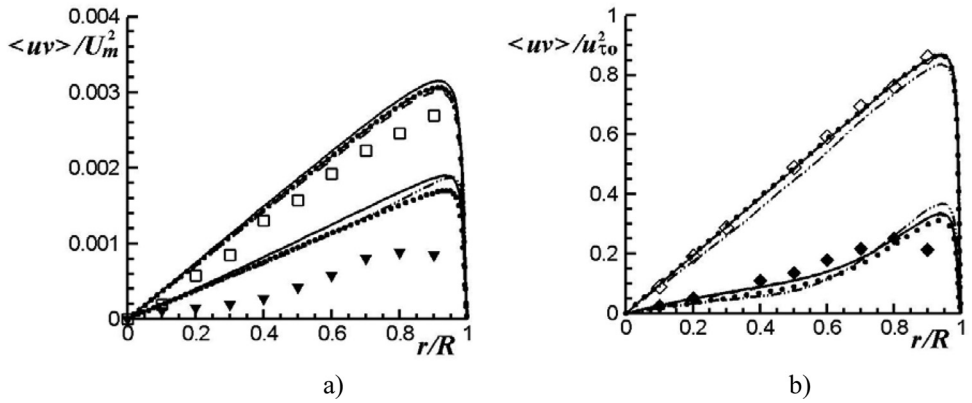

Fig. 6 Shear stress at (*a*) $Re = 2\times10^4$ and (*b*) $Re = 4\times10^4$ (see notations in Fig. 4)

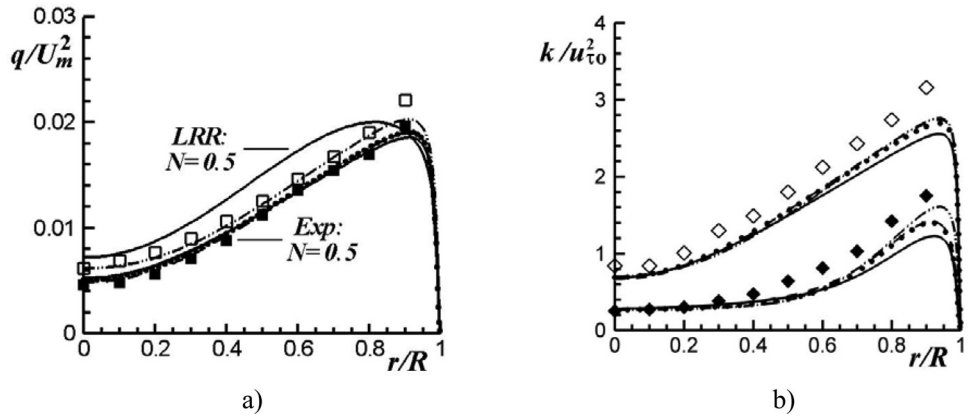

Fig. 7 Turbulent kinetic energy (*a*) $Re = 2\times10^4$ and (*b*) $Re = 4\times10^4$ (see notations in Fig. 4)

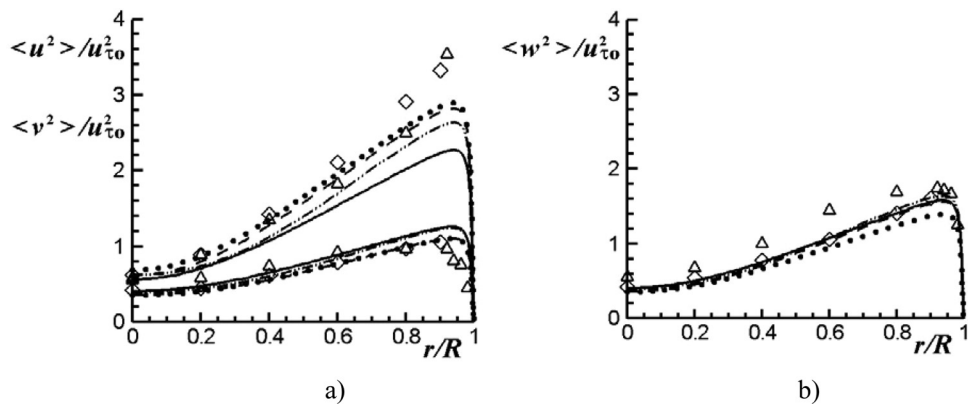

Fig. 8 The individual components of turbulent kinetic energy at the exit of the stationary pipe section at $Re = 4\times10^4$ for: (*a*) $\langle u^2\rangle/u_{\tau o}^2$ (upper lines), $\langle v^2\rangle/u_{\tau o}^2$ (lower lines) and (*b*) $\langle w^2\rangle/u_{\tau o}^2$. Notations: —· LRR model, - - - - LSSG model, ····· SSG model, — ··— Q-model; experiments: [25], *r* [28].

only at $N = 0$. Wall corrections in the models do not solve this problem [10,13], but using a tensor-invariant model for turbulent diffusion resolves the issue [10].

In the stationary pipe section at $\mathrm{Re} = 2 \times 10^4$, the Q-model more accurately predicts the turbulent kinetic energy profile than the other models (Fig. 7(*a*)). In this figure, $q = 2k$. By using wall corrections in this model, overall results can be improved in the near-wall region. Other models underpredict the turbulent kinetic energy level at any r. Wall corrections will not be sufficient to improve simulation results.

At higher Reynolds numbers, the four models generate similar solutions. That is, they all underpredict the turbulent kinetic

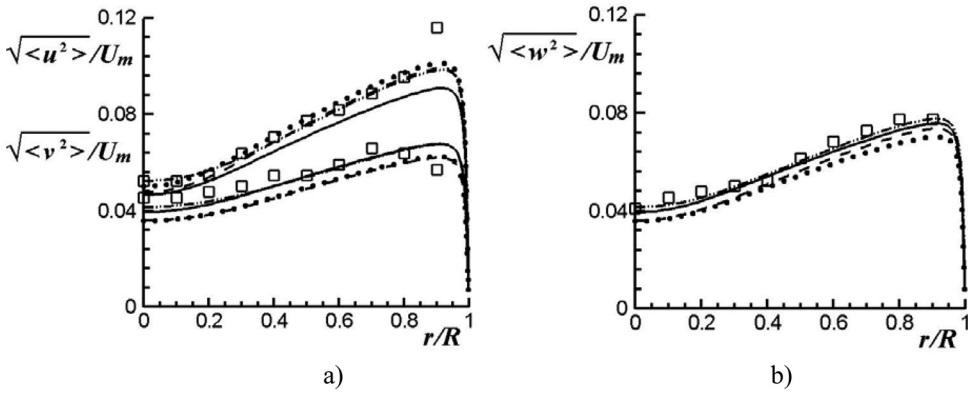

Fig. 9 Individual components of the turbulent kinetic energy at the exit of the stationary pipe section at $Re = 2\times10^4$ for: (*a*) $\sqrt{\langle u^2\rangle}/U_m$ (upper lines), $\sqrt{\langle v^2\rangle}/U_m$ (lower lines) and (*b*) $\sqrt{\langle w^2\rangle}/U_m$. Notations: —- LRR model, - - - - LSSG model, ····· SSG model, – ·–· Q-model; experiments: □ [27].

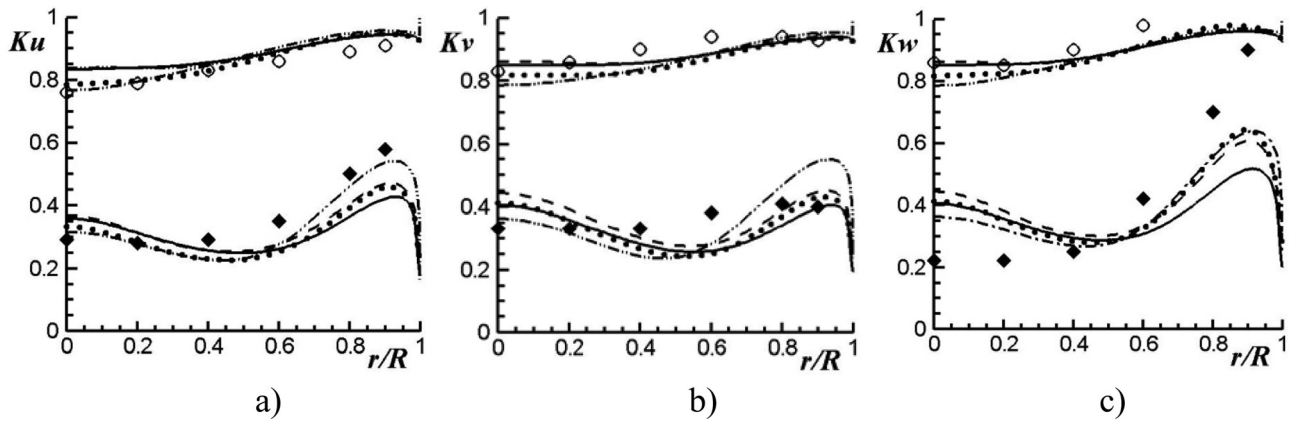

Fig. 10 Effect of rotation on the individual components of turbulent kinetic energy at $Re = 4\times10^4$ (see notations in Fig. 4)

energy level near the wall (Fig. 7(*b*)). Under rotation, the Q-model produces the k-profile in close agreement with the experimental data, including the near-wall area.

The individual components of turbulent kinetic energy at the exit of the stationary pipe section are shown in Figs. 8 and 9. Experimental data from Ref. [28] are plotted in Fig. 8 along with experimental data from Refs. [25] and [27] and computational profiles, in order to provide more detailed information about the flow behavior near the pipe wall. In Ref.[28], the data were obtained at $\mathrm{Re} = 5 \times 10^4$. Therefore, the data can be used only for a qualitative comparison.

At $\mathrm{Re} = 4 \times 10^4$, all models under-predict $\langle u^2\rangle$ and $\langle v^2\rangle$ in the near-wall area (Fig. 8). The LRR-model profile of $\langle u^2\rangle$ deviates from the experimental data at any r. The SSG model underpredicts the level of $\langle w^2\rangle$ at any r, whereas the other three models provide an accurate prediction of this component. Figure 9 shows similar tendencies. Both figures demonstrate that $\langle u^2\rangle$ is the most challenging Reynolds stress to predict.

Rotation influences the individual components of the turbulent kinetic energy in a manner similar to the effect of rotation on their sum. That is, at a lower Re, all components are significantly overpredicted (not shown here). At a higher Re and small N ($N = 0.15$), there is an acceptable agreement with the experimental data, including in the near-wall area (Fig. 10). In the figure, Ku, Kv, and Kw are damping coefficients defined as

$$Ku_i = \frac{\langle u_i^2\rangle(N>0)}{\langle u_i^2\rangle(N=0)}, \text{ where } u_i = u,\ v,\ \text{or } w$$

Under stronger rotation, $\langle u^2\rangle$ and $\langle v^2\rangle$ are reproduced in close agreement with the experimental profiles, whereas $\langle w^2\rangle$ is the most challenging to predict for all models (Fig. 10). Clearly, wall corrections will not improve these results.

5 Conclusions

Results of the present study demonstrate that the IP model is too simplified to be used in test flow without adding corrections to pressure-strain models. The other four RST models tested in the present study were able to capture the flow physics significantly better. Profiles of the mean velocity components that were calculated without wall corrections were in agreement with the experimental data. Different models produce close results, but at $\mathrm{Re} = 2 \times 10^4$, the circumferential mean velocity component profiles that were calculated with the Q-model deviate far from experimental data and show the wrong tendency towards flow relaminarization. With increasing the Reynolds number, the difference between the profiles calculated for the different models becomes negligible at considered rotation rates.

Calculation of the $\langle uv\rangle$ profile for the four models does not require wall corrections at higher Re. The deviation from experimental data that occurred near walls can be corrected using a tensor-invariant model for the turbulent diffusion, rather than model (3) utilized in the current study [10]. Whether this substitution would be sufficient to improve the solution for this Reynolds stress at a lower Re is not currently clear. However, the use of wall corrections will certainly not resolve the issue, as the

simulation results deviate from the experimental data at any r, not only in the near-wall area.

The choice of a model for turbulent diffusion is also important for predicting turbulent kinetic energy at a lower Re. With a gradient-diffusion-type model such as model (3), all considered RST models overpredict the turbulent kinetic energy level in the fully developed turbulence region of the rotating pipe section. Moreover, they predict it to be larger than in the stationary pipe. This contradicts experimental observations.

In the stationary pipe section, all models underpredict the level of turbulent kinetic energy near the pipe wall at both Reynolds numbers. Under rotation at a higher Re, the Q-model gives results close to the experimental data, including in the near-wall area. Other models underpredict the level of turbulent kinetic energy near the wall.

The individual components of the turbulent kinetic energy behave differently when under rotation and in the near-wall area. The LRR model has more difficulties reproducing these differences than other models. The SSG model completely fails under strong rotation ($N = 1$), predicting flow relaminarization. Other models also predict flow relaminarization in contradiction to experimental observations, but this occurs at higher rotation rates. Overall, the LSSG model without wall corrections produces the best results in the tested flow within considered ranges of the flow parameters.

The Reynolds number and the rotation rate have similar effects on the accuracy of simulation results. By increasing either of these parameters (excluding strong rotation), results of simulations tend to be in closer agreement with experimental data, including in the near-wall area.

Acknowledgment

Initial data for this study was obtained by the author when she was affiliated with the Center for Turbulence Research, Stanford University. A portion of the research was conducted under NASA Cooperative Agreement NNX12AJ61A.

References

[1] Monin, A. S., and Yaglom, A. M., 1979, *Statistical Fluid Mechanics: Mechanics of Turbulence*, Vol. 1, The MIT Press, Cambridge, MA, Chap. 4.
[2] Lumley, J. L., 1975, "Introduction," *Lecture Series 76, Prediction Methods for Turbulent Flows*, von Kármán Institute for Fluid Dynamics, Rhode-St-Genese, Belgium.
[3] Rumsey, C. L., Gatski, T. B., Sellers III, W. L., Vatsa, V. N., and Viken, S. A., 2004, "Summary of the 2004 CFD Validation Workshop on Synthetic Jets and Turbulent Separation Control," Proc. 2nd AIAA Flow Control Conference, AIAA-2004-2217,.
[4] Johansson, T. G., and Davidson, L., 2006, "The 11th ERCOFTAC Workshop on Refined Turbulence Modelling," the Czestochowa University of Technology, Czestochowa, Poland, ERCOFTAC Bulletin, 69-2006.
[5] Thiele, F., and Jakirlic, S., 2007, "The 12th ERCOFTAC/IAHR/COST Workshop on Refined Turbulence Modelling," the Czestochowa University of Technology, Czestochowa, Poland, ERCOFTAC Bulletin, 75-2007.
[6] Torii, S., and Yang, W., 1995, "Numerical Prediction of Fully Developed Turbulent Swirling Flows in an Axially Rotating Pipe by Means of a Modified k-ε Turbulence Model," Int. J. Numer. Meth. Heat Fluid Flow, **5**, pp. 175–183.
[7] Hanjalić, K., and Launder, B., 2011, *Modelling Turbulence in Engineering and the Environment*, Cambridge University Press, Cambridge, UK.
[8] Kurbatskii, A. F., Poroseva, S. V., and Yakovenko, S. N., 1995, "Calculation of Statistical Characteristics of a Turbulent Flow in a Rotating Cylindrical Pipe," High Temp., **33**(5), pp. 738–748.
[9] Kurbatskii, A. F., and Poroseva, S. V., 1997, "A Model for Calculating the Three Components of the Excess for the Turbulent Field of Flow Velocity in a Round Pipe Rotating About Its Longitudinal Axis," High Temp., **35**(3), pp. 432–440.
[10] Kurbatskii, A. F., and Poroseva, S. V., 1999, "Modelling Turbulent Diffusion in a Rotating Cylindrical Pipe Flow," Int. J. Heat Fluid Flow, **20**(3), pp. 341–348.
[11] Daly, B. J., and Harlow, F. H., 1970, "Transport Equations in Turbulence," Phys. Fluids, **13**, pp. 2634–2649.
[12] So, R. M. C., and Yoo, G. J., 1986, "On the Modeling of Low-Reynolds-Number Turbulence," NASA CR 3994.
[13] Poroseva, S. V., Kassinos, S. C., Langer, C. A., and Reynolds, W. C., 2002, "Structure-Based Turbulence Model: Application to a Rotating Pipe Flow," Phys. Fluids, **14**(4), pp. 1523–1532.
[14] Kassinos, S. C., Langer, C. A., Haire, S. L., and Reynolds, W. C., 2000, "Structure-Based Turbulence Modeling for Wall–Bounded Flows," Int. J. Heat Fluid Flow, **21**, pp. 599–605.
[15] Rotta, J. C., 1951, "Statistische Theorie Nichthomogener Turbulenz," Z. Phys., **129**, pp. 547–572; 131, pp. 51–77.
[16] Poroseva, S. V., 2001, "Modeling the "Rapid" Part of the Velocity/Pressure-Gradient Correlation in Inhomogeneous Turbulence," Annual Research Brief 2001, Center for Turbulence Research, NASA-Ames/Stanford University, pp. 367–374.
[17] Poroseva, S. V., 2000, "New Approach to Modeling the Pressure-Containing Correlations," Proc. of the 3rd Inter. Symposium on Turbulence, Heat and Mass Transfer, Nagoya, Japan, pp. 487–493.
[18] Poroseva, S. V., and Iaccarino, G., 2001, "Simulating Separated Flows Using the k-ε Model," Annual Research Brief 2001, Center for Turbulence Research, NASA-Ames/Stanford Univ., pp. 375–384.
[19] Launder, B. E., Reece, G. J., and Rodi, W., 1975, "Progress in Development of a Reynolds-Stress Turbulent Closure," J. Fluid Mech., **68**, pp. 537–566.
[20] Gatski, T. B., and Speziale, C. G., 1993, "On Explicit Algebraical Stress Models for Complex Turbulent Flow," J. Fluid Mech., **254**, pp. 59–78.
[21] Speziale, C. G., Sarkar, S., and Gatski, T. B., 1991, "Modeling the Pressure-Strain Correlation of Turbulence: An Invariant Dynamical System Approach," J. Fluid Mech., **227**, pp. 245–272.
[22] Kassinos, S. C., Reynolds, W. C., and Rogers, M. M., 2001, "One-Point Turbulence Structure Tensors," J. Fluid Mech., **428**, pp. 213–248.
[23] Spalding, D. B., 1977, *GENMIX: A General Computer Program for Two-Dimensional Parabolic Phenomena*, Pergamon, New York.
[24] Kikuyama, K., Murakami, M., Nishibori, K., and Maeda, K., 1983, "Flow in an Axially Rotating Pipe (a Calculation of Flow in the Saturated Region)," Bull. JSME, **26**, pp. 506–513.
[25] Zaets, P. G., Safarov, N. A., and Safarov R. A. 1985, "Experimental Study of the Behavior of Turbulence Characteristics in a Pipe Rotating Around Its Axis," Modern Problems of Continuous Medium Mechanics, Moscow Physics and Technics Institute, Moscow, Russia, pp. 136–142 (in Russian).
[26] Nishibori, K., Kikuyama, K., and Murakami, M., 1987, "Laminarization of Turbulent Flow in the Inlet Region of an Axially Rotating Pipe," Bull. JSME, **30**, pp. 255–262.
[27] Imao, S., Itoh, M., and Harada, T., 1996, "Turbulent Characteristics of the Flow in an Axially Rotating Pipe," Int. J. Heat Fluid Flow, **17**, pp. 444–451.
[28] Laufer, J., 1954, "The Structure of Turbulence in Fully Developed Pipe Flow," NASA Report 1174.